Physics in Medicine & Biology





RECEIVED

3 October 2022

REVISED

26 December 2022

ACCEPTED FOR PUBLICATION 18 January 2023

PUBLISHED 6 February 2023

PAPER

In vivo estimation of anisotropic mechanical properties of the gastrocnemius during functional loading with MR elastography

Daniel R Smith^{1,2,3}, Diego A Caban-Rivera¹, L Tyler Williams¹, Elijah E W Van Houten⁴, Phil V Bayly⁵, Keith D Paulsen^{6,7}, Matthew D J McGarry⁶ and Curtis L Johnson^{1,*}

- ¹ Department of Biomedical Engineering, University of Delaware, 19711, Newark DE, United States of America
- ² Department of Orthopaedics, Emory University School of Medicine, 30307, Atlanta GA, United States of America
- ³ Emory Sports Performance and Research Center, Flowery Branch GA, 30542, United States of America
- ⁴ Université de Sherbrooke, Sherbrooke, QC, J1K 2R1, Canada
- Department of Mechanical Engineering and Materials Science, Washington University in St. Louis, St. Louis MO, United States of America
- ⁶ Thayer School of Engineering, Dartmouth College, 03755, Hanover NH, United States of America
- Dartmouth-Hitchcock Medical Center, 03756, Lebanon NH, United States of America
- * Author to whom any correspondence should be addressed.

E-mail: clj@udel.edu

Keywords: magnetic resonance elastography, skeletal muscle, stiffness, tension, gastrocnemius

Abstract

Objective. In vivo imaging assessments of skeletal muscle structure and function allow for longitudinal quantification of tissue health. Magnetic resonance elastography (MRE) non-invasively quantifies tissue mechanical properties, allowing for evaluation of skeletal muscle biomechanics in response to loading, creating a better understanding of muscle functional health. Approach. In this study, we analyze the anisotropic mechanical response of calf muscles using MRE with a transversely isotropic, nonlinear inversion algorithm (TI-NLI) to investigate the role of muscle fiber stiffening under load. We estimate anisotropic material parameters including fiber shear stiffness (μ_1), substrate shear stiffness (μ_2), shear anisotropy (ϕ), and tensile anisotropy (ζ) of the gastrocnemius muscle in response to both passive and active tension. Main results. In passive tension, we found a significant increase in μ_1 , ϕ , and ζ with increasing muscle length. While in active tension, we observed increasing μ_2 and decreasing ϕ and ϕ during active dorsiflexion and plantarflexion—indicating less anisotropy—with greater effects when the muscles act as agonist. Significance. The study demonstrates the ability of this anisotropic MRE method to capture the multifaceted mechanical response of skeletal muscle to tissue loading from muscle lengthening and contraction.

1. Introduction

Non-invasive evaluation of skeletal muscle health *in vivo* allows for longitudinal assessments of tissue structure and function. Primary assessment tools include measurement of muscle activation through surface electromyography (sEMG) (Komi and Viitasalo 1976, Kellis and Baltzopoulos 1998, Raiteri *et al* 2016), and imaging of tissue structure with ultrasound imaging (Pillen and van Alfen 2011, van Hooren *et al* 2020, Naruse *et al* 2022) and magnetic resonance imaging (MRI) (Murphy *et al* 1986, Díaz-Manera *et al* 2015). These techniques each have their advantages, with sEMG and ultrasound imaging providing high temporal resolution during muscle activation, while MRI provides a large field-of-view (FOV) to better investigate multiple muscles and their interactions simultaneously. An additional benefit of MRI is the ability to more comprehensively examine the complex structure of skeletal muscle by combining standard MRI contrasts, such as T1-weighted (Shen *et al* 2013, Kalia *et al* 2017, Marty and Carlier 2019) and T2-weighted (Johnston *et al* 2015, Yao *et al* 2016, Biglands *et al* 2020) imaging, with quantitative contrasts sensitive to tissue biophysics, such as diffusion tensor imaging (DTI) (Sinha *et al* 2006, Schwenzer *et al* 2009, Oudeman *et al* 2016) and MR spectroscopy (Boesch *et al* 1997, Deshmukh *et al* 2014).

One such MRI modality is magnetic resonance elastography (MRE), which is a phase-contrast technique that measures propagating time-harmonic shear waves to probe the mechanical properties of tissues and has been successfully used to analyze the health of other human organs (Mariappan et al 2010, Litwiller et al 2012, Hiscox et al 2016, Bayly and Garbow 2018). In skeletal muscle, MRE has shown to capture changes in tissue mechanical properties reflecting muscle microstructure due to aging (Debernard et al 2011, Kennedy et al 2020), exercise (Green et al 2012, Kennedy et al 2017), and pathology, including Duchenne muscle dystrophy (Basford et al 2002, Ringleb et al 2007, Bensamoun et al 2015). MRE has also shown to reflect muscle activation through changes in the apparent mechanical stiffness of the tissue. In particular, (Zonnino et al 2019) quantified the effects of variable isometric contraction on MRE estimates in the human forearm, as well as how changing muscle length affected the responses of those muscles. Additionally, (Schrank et al 2020) used a real-time MRE method to quantify parameter changes in calf muscles during isometric contraction loading conditions. In these examples, muscles appeared stiffer during contraction, indicating an avenue to better understand muscle force output.

While previous studies have demonstrated the potential of MRE for characterizing skeletal muscle, they have largely employed isotropic material models when estimating tissue mechanical properties, which are then susceptible to inaccuracies given the fibrous composition of muscle that leads to anisotropic mechanical behavior (Guidetti et al 2019, Palnitkar et al 2019). Several recent MRE studies of skeletal muscle have attempted to incorporate mechanical anisotropy, including works by Green et al (2013), Guo et al (2016), and Babaei et al (2021). These studies each modeled muscle as an incompressible, transversely isotropic tissue with two anisotropic shear parameters defining the tissue response to shear deformations parallel and perpendicular to the muscle fibers. Fiber stretching, a critical component of the mechanical response of muscle during contraction, cannot be represented by two shear parameters alone, and instead requires an additional parameter to capture the tensile mechanical response. Recently, a nearly incompressible, transversely isotropic (NITI) material model, which incorporates three parameters to describe the tissue—substrate shear stiffness, shear anisotropy, and tensile anisotropy—has shown promise in modeling both the shear and tensile components of anisotropy in fibrous human tissue when combined with MRE displacement data (Feng et al 2013, Tweten et al 2015, 2017, Smith et al 2020, 2022). Through estimation of the three independent mechanical property parameters, the NITI material model provides an effective framework from which to quantify the mechanical response of skeletal muscle as it is functionally activated.

Most studies analyzing the link between measurements of anisotropic mechanical properties of skeletal muscle and tissue structure and function have utilized *ex vivo* techniques and have shown significant variations in tissue mechanical response during both passive stretching and active contraction (Huijing 1999, Wheatley 2020). These prior works have characterized muscle force production and transmission in both the axial and lateral directions (Ramaswamy *et al* 2011, Mohammadkhah *et al* 2018, Maas 2019), with greater axial loading in the direction of the muscle fibers occurring during passive stretching, while active contraction produces higher forces in the lateral direction (Böl 2009, Takaza *et al* 2013). Capturing these variations in muscle mechanics *in vivo* would allow for more accurate assessments of skeletal muscle functional responses that incorporate the entire muscle volume, and other muscles and bone that make up the lower leg. Additionally, it would establish MRE as sensitive to tissue structure and function to allow for the assessment of longitudinal effects of injury and pathology in individual subjects.

Therefore, the purpose of this study is use MRE to capture anisotropic mechanical behavior in skeletal muscle *in vivo* consistent to previous *ex vivo* studies. To test this, we estimated the anisotropic mechanical properties of skeletal muscle using the recently developed transversely isotropic, nonlinear inversion algorithm (TI-NLI) that incorporates wave motion fields from MRE with fiber orientation data acquired with diffusion tensor imaging (DTI) (McGarry *et al* 2021a, 2022). We performed two experiments to probe the mechanical reaction of skeletal muscle: the first to investigate passive contraction through muscle stretching, and the second to explore the mechanical variations caused by active isometric contraction.

2. Methods

2.1. Experimental setup

Eight healthy young adult subjects (4/4 M/F; ages 23–26) completed the study approved by our Institutional Review Board. All participants were imaged in a Siemens 3T Prisma MRI scanner. Each subject was positioned supine, feet first in the bore with legs draped over an adjustable support as shown in figure 1. Two RF receiver coils were wrapped around the calf with two custom-made passive drivers to generate the necessary shear waves for MRE in conjunction with the Resoundant pneumatic actuation system. For Experiment 1, the right ankle of each subject was placed in a custom brace to limit range of motion while the height of the knee was adjusted to achieve three different angles: 105°, 135°, and 165°. For Experiment 2, the right foot of each subject was

Phys. Med. Biol. **68** (2023) 045004 D R Smith et al

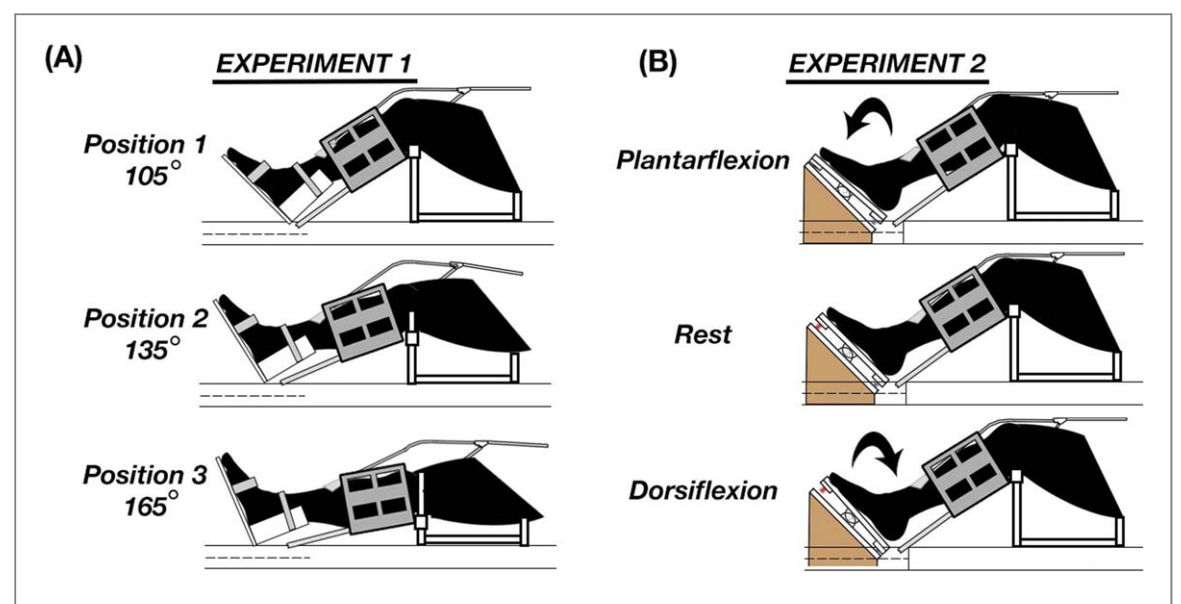


Figure 1. (A) Experiment 1 entailed placing the subject's foot in a custom ankle brace to maintain a constant ankle angle while the angle of subject's knee was altered through raising or lowering the leg support. (B) Experiment 2 replaces the ankle brace with a pedal-like device which induced isometric contraction when the subject pushed against one of the two springs during dorsi- or plantar-flexion, while the leg was supported at a constant knee angle.

positioned on a pedal device. Individuals were instructed to press and hold down one side of the footplate to compress fully one of the plastic springs, as illustrated in figure 1(B), for the duration of each MRE scan. This positioning induced isometric dorsi- or plantar-flexion depending on which spring the subject compressed. Subjects practiced these movements prior to scanning to acclimate themselves to the force required to minimize variability between participants and acquisitions.

2.2. Imaging protocol

MRE data was collected using an echo-planar imaging (EPI) sequence with the following parameters: $2 \times 2 \times 3$ mm³ voxel size; FOV = 160×160 mm; 80×80 matrix; 20 slices with 3 mm thickness; repetition time (TR)/ echo time (TE) = 2400/59 ms; vibration frequency = 50 Hz; 4 phase offsets; dual gradient polarity; total acquisition time = 65 s. Thicker slices were used to increase signal-to-noise ratio, and were positioned axially where anatomical features and mechanical properties are assumed to vary more slowly along the leg. We also acquired a diffusion tensor imaging (DTI) scan with resolution and FOV matched to the MRE data with TR/ TE = 2200/69 ms, b = 400 s mm⁻² and 30 directions, as well as a T1-weighted scan with the following parameters: $1.25 \times 1.25 \times 3$ mm³ voxel size; FOV = 160×160 mm; 128×128 matrix; 20 slices; TR/ TE = 2200/11 ms;

Each subject completed both Experiment 1 and Experiment 2 within the same scanning session. Experiment 1 consisted of a set of image acquisitions at each of three knee angles (105°, 135°, and 165°). At each position, we collected three repeated MRE scans, one DTI scan, and one T1-weighted anatomical scan. Experiment 2 consisted of three repeated MRE acquisitions during each contraction condition—dorsi-flexion, plantar-flexion, and rest—for a total of nine MRE scans. Additionally, we acquired one DTI scan and one T1-weighted anatomical scan as in Experiment 1. All imaging volumes were manually aligned to be axial to the leg for different leg positions in both experiments.

2.3. Data processing

Diffusion data was processed with the FMRIB's Diffusion Toolbox (FDT) from FMRIB's Software Library (FSL) (Jenkinson $et\,al\,2012$). We then used FMRIB's Linear Image Registration Tool (FLIRT) to register the diffusion-weighted images with MRE image space using the diffusion gradient directions for each image rotated according to the registration. From there, fractional anisotropy and the first eigenvector (V_1) were calculated using FDT.

Wave motion fields were calculated from MRE data after subtraction to remove background phase, phase unwrapping with FSL PRELUDE (Jenkinson 2003), and temporal Fourier filtering to isolate the harmonic motion of interest. We then used a transversely isotropic, nonlinear inversion algorithm (TI-NLI) to estimate anisotropic material parameters based on the acquired wave motion fields and the primary eigenvector from DTI, the assumed fiber direction (McGarry et al 2021a, 2022), as shown in figure 2. TI-NLI is an iterative, finite element-based inversion that estimates spatial maps of the three material property parameters used to describe a NITI model: substrate shear modulus, G_2 , shear anisotropy, $\phi = |G_1|/|G_2| - 1$, and tensile anisotropy,

Phys. Med. Biol. **68** (2023) 045004 D R Smith et al

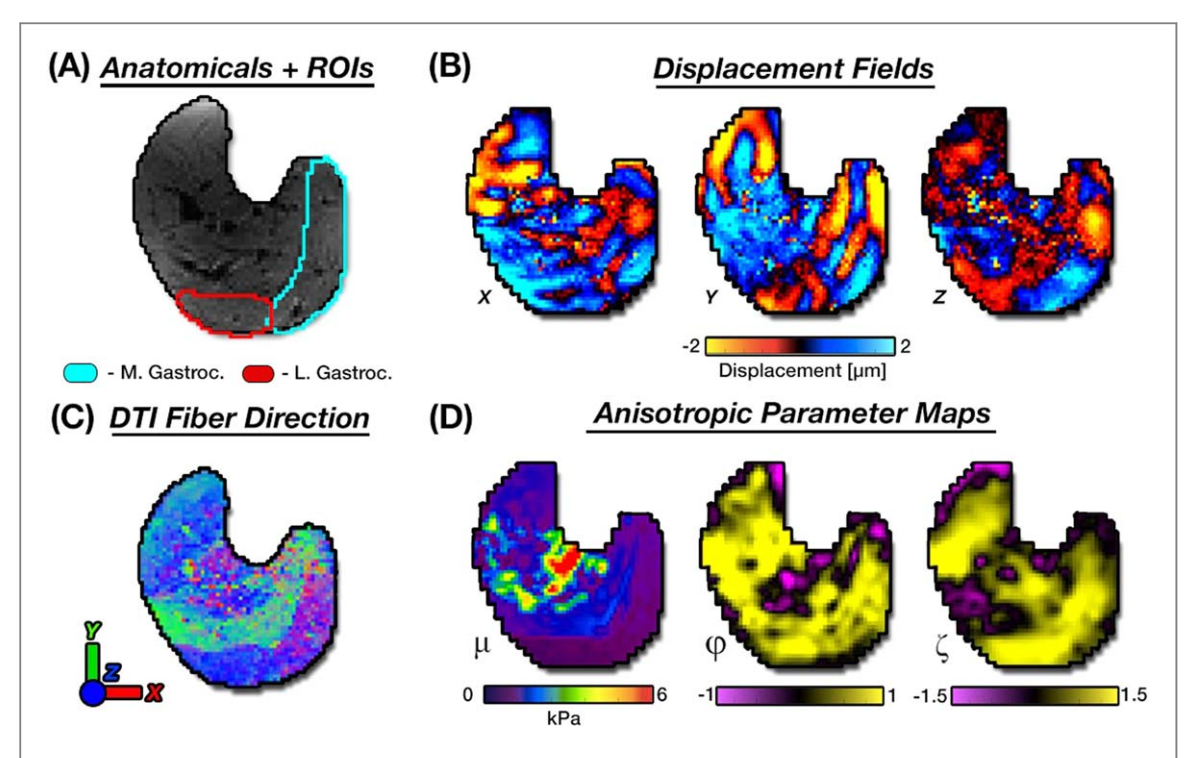


Figure 2. (A) Two primary muscles, medial and lateral heads of the gastrocnemius, were investigated to determine anisotropic material parameters. Three material property parameters were estimated by combining (B) MRE displacement fields with (C) DTI fiber directions. The anisotropic parameters included (D) substrate shear stiffness (μ), shear anisotropy (ϕ), and tensile anisotropy (ζ).

 $\zeta = |E_1|/|E_2| - 1$, where G and E are defined as a material shear and tensile moduli respectively. Subscript 1 denotes a property parallel to the direction of the fiber, or normal to the plane of isotropy, while a subscript 2 denotes a property perpendicular to the fiber direction, or in the plane of isotropy. The substrate shear modulus is defined by the equation: $G_2 = G_2' + iG_2''$, where G_2' is the substrate storage modulus, and G_2'' , is the substrate loss modulus. Here we calculate the substrate shear stiffness as $\mu_2 = \frac{2 \mid G_2 \mid^2}{G_2' + \mid G_2 \mid}$, which describes the square of the wave speed perpendicular to the fibers. We also considered the shear stiffness parallel to the fibers as $\mu_1 = \mu_2(1 + \phi)$. We note that the parameters estimated in this study are 'effective' mechanical properties due to the nonlinear acoustoelastic effects of the pre-strain fields on the skeletal muscle (Abiza *et al* 2012).

We estimated the average anisotropic properties in individual calf muscles, specifically the medial and lateral heads of the gastrocnemius, which were manually traced from anatomical images. Within TI-NLI, we applied soft prior regularization using these generated volumes as *a priori* spatial information to stabilize the estimation of properties (McGarry *et al* 2013). To analyze differences in muscle parameters between contraction states, we applied a linear mixed model with variables of muscle, subject, and position as fit parameters for Experiment 1, and a one-way ANOVA with repeated measures within subject and muscle with relationships between a post-hoc Tukey test for Experiment 2.

3. Results

3.1. Experiment 1—passive muscle lengthening

Figure 3 displays results from Experiment 1 and shows changes in the anisotropic material parameters in the gastrocnemii when placed in the three knee positions: 105° , 135° , and 165° . Associated descriptive statistics are summarized in table 1. We found increases in μ_1 , ϕ , and ζ as knee angle increases (each p < 0.05), while μ_2 stayed relatively stable. Using data from both muscles individually, μ_1 increased by approximately 7.6% overall, from 1.66 to 1.79 kPa, between the initial and final position (p = 0.061). ϕ , however, increased 7.6% between a knee angle of 105° and 135° and 1.8% between a knee angle of 135° and 165° , for a total increase of 9.5% from 0.30 to 0.33 (p < 0.05). ζ exhibited similar increases the three knee positions—38% between a knee angle of 105° and 135° and 1

3.2. Active muscle contraction

Figure 4 highlights the anisotropic parameter estimates of gastrocnemius during isometric contraction in dorsiflexion and plantar-flexion relative to rest from Experiment 2. Associated descriptive statistics are summarized

Phys. Med. Biol. **68** (2023) 045004 D R Smith et al

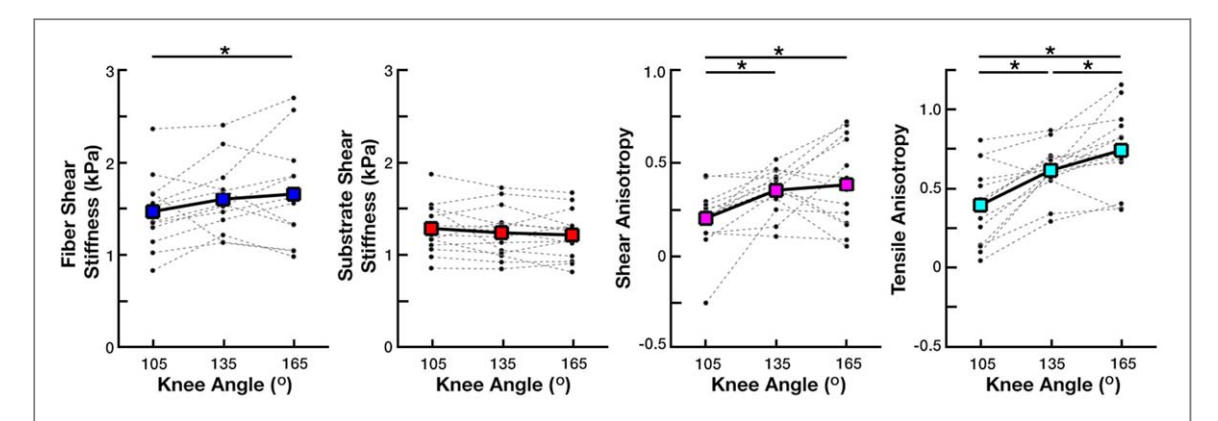


Figure 3. Results from Experiment 1 comparing the effects of increasing muscle length with knee angle on fiber shear stiffness, substrate shear stiffness, shear anisotropy, and tensile anisotropy (left to right) in both heads of the gastrocnemius muscle. Statistically significant differences are denoted by *.

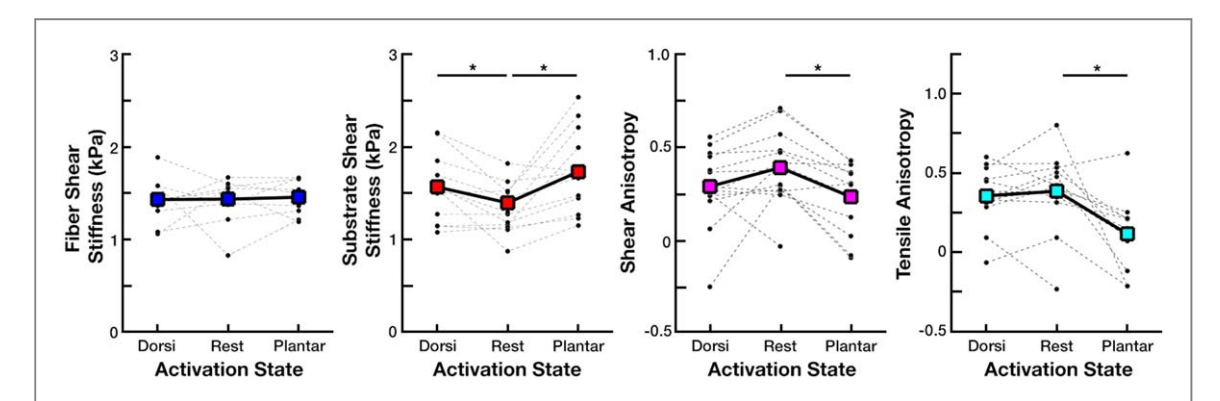


Figure 4. Results from Experiment 2 comparing the effects of isometric contraction on fiber shear stiffness, substrate shear stiffness, shear anisotropy, and tensile anisotropy (left to right) in both heads of the gastrocnemius muscle. Statistically significant differences are denoted by *.

Table 1. Average and standard deviations of four mechanical property parameters at the three knee angles measured during Experiment 1.

	μ_1 (kPa)	μ_2 (kPa)	φ	ζ
105°	1.49 ± 0.41	1.28 ± 0.27	0.20 ± 0.17	0.40 ± 0.24
135°	1.62 ± 0.40	1.23 ± 0.27	$\boldsymbol{0.35 \pm 0.12}$	$\boldsymbol{0.62 \pm 0.16}$
165°	$\boldsymbol{1.67 \pm 0.57}$	$\boldsymbol{1.21 \pm 0.26}$	$\boldsymbol{0.38 \pm 0.24}$	$\boldsymbol{0.74 \pm 0.25}$

in table 2. Here, the parameters— μ_2 , ϕ , and ζ —exhibited significant changes between the contraction states (p < 0.05), while μ_1 was relatively stable. From the rest condition, μ_2 increased from 1.39 to 1.56 kPa during dorsiflexion (p < 0.05) and to 1.73 kPa during plantarflexion (p < 0.05), increases of 20% and 13%, respectively. ϕ and ζ had opposite responses, instead showing non-significant decreases from 0.13 to 0.03 (34.6%; p = 0.106) and 0.39 to 0.36 (6.9%; p = 0.72) during dorsiflexion, respectively, and significant decreases from 0.13 to -0.02 (66.7%; p < 0.05) and 0.39 to 0.12 (67.5%; p < 0.05) during plantarflexion.

4. Discussion

In this study, we used MRE to capture the mechanical response occurring in skeletal muscle during isometric contraction and passive lengthening, specifically captured variations in anisotropic mechanical properties of the medial and lateral heads of the gastrocnemius muscle. Most *in vivo* evaluations of anisotropic mechanical properties of skeletal muscle quantify the resting state shear stiffness and shear anisotropy. In this study, measurements of shear stiffness and shear anisotropy were relatively similar to results from previous reports in the MRE literature with similar vibration frequencies ($\mu_1 = 1.26 - 1.32$ kPa , $\mu_2 = 1.53 - 2.00$ kPa, and $\phi = 0.18 - 0.59$) (Green *et al* 2013, Guo *et al* 2016, Babaei *et al* 2021). The repeatability of the estimated shear moduli were

Table 2. Average and standard deviations of four mechanical property parameters at the three different active contraction states measured during Experiment 2.

	μ_1 (kPa)	μ_2 (kPa)	φ	ζ
Dorsiflexion	1.43 ± 0.29	1.56 ± 0.36	0.03 ± 0.20	0.36 ± 0.18
Rest	1.43 ± 0.38	1.39 ± 0.30	0.13 ± 0.19	$\boldsymbol{0.39 \pm 0.24}$
Plantarflexion	$\boldsymbol{1.45 \pm 0.19}$	$\boldsymbol{1.73 \pm 0.45}$	-0.02 ± 0.19	$\textbf{0.12} \pm \textbf{0.23}$

within the range of previous MRE studies, with the coefficient of variation, defined as $\frac{\text{Mean}}{\text{St. Dev.}}$, for the repeated measurements of a single subject averaging 5.0% in experiment 1 and 10.9% in experiment 2 (Johnson *et al* 2013, Smith *et al* 2022). None of the prior published studies reported ζ as a material parameter; hence, comparisons were not possible with the data presented here. In previous studies, MRE-measurements of calf muscles have utilized large knee angles with a nearly-straight leg and a non-flexed ankle, most similarly to our Position 3 at 165° knee angle during Experiment 1. The TI-NLI employed in this study has been demonstrated to accurately recover μ , ϕ and ζ images using realistic simulated data which supports the accuracy of our measurements (McGarry *et al* 2021a, McGarry 2022).

In Experiment 1, we showed the degree of anisotropic parameter change during alterations in passive tension on a muscle through changes in muscle length. The gastrocnemius is the only dual-joint muscle in the calf, meaning it crosses both knee and ankle joints. Therefore, by limiting the motion of the ankle, we can alter the length and pennation angle of the gastrocnemius by changing knee angle and increase the length of the sarcomeres within the muscle fibers (Riemann et al 2001, Maganaris 2003). Previous literature has shown that this increases in muscle length also increases the applied load on the muscle fibers (Evans and Hill 1914, Gordon et al 1966, Kaufman et al 1989). This outcome is reflected in results from Experiment 1, where μ_1 , the shear stiffness in planes parallel to the fiber direction, increased with increasing knee angle. One of the primary drivers of this increased stiffness and anisotropy is likely the stretching of collagen-based structures within the muscle, including epimysium, perimysium, and endomysium as well as the muscle fiber extracellular matrix, resulting in higher levels of pre-stress and pre-strain within the tissue (Stecco et al 2021). As these collagen structures are stretched, the collagen becomes more highly aligned (Gillies and Lieber 2011, Csapo et al 2020), which has also been reflected in diffusion imaging studies (Schwenzer et al 2009, Oudeman et al 2016). The pathway for the increase in tension is likely also related to titin, the third structural protein within sarcomeres which studies suggest causes passive force enhancement (Herzog et al 2012, 2015). Titin primarily acts as a molecular spring with the ability to alter stiffness during muscle activation to maintain stability in muscles that are stretched to long lengths. Previous ex vivo studies have also shown that muscle fibers and their sarcomeres produce low levels of lateral forces during muscle lengthening (Böl 2009, Mohammadkhah et al 2018), though in this work we observed no significant change in μ_2 during passive muscle lengthening, suggesting that the mechanism of lateral force creation may not be significant enough to be detected via changes in substrate stiffness.

In a previous MRE study of skeletal muscle, (Babaei $et\,al\,2021$) found a similar relationship between μ_1 and muscle length, though results differed for μ_2 and ϕ , as μ_2 significantly increased while ϕ stayed relatively stable as the muscle stretched. One possible reason for differences in these results is the different material models used in the two studies. Babei $et\,al$ assumed tissue incompressibility with only the presence of slow propagating shear waves, and accordingly, no fast propagating shear wave effects (i.e. only shear anisotropy and no tensile anisotropy). Ignoring the fast shear wave component in skeletal muscle may bias estimates of shear moduli, since fast waves are likely to be present in an NITI material unless care is taken to avoid their excitation (Tweten $et\,al\,2015$). Under the assumption of full incompressibility, tissue stretching must be represented in other measurements, possibly resulting in the mismatch in outcomes between the two studies. Another possible explanation could be the lack of knee restraint in the Babei study. As previously noted, the gastrocnemius muscle can be stretched or shortened by changing the angle of either the ankle or knee; hence, while the ankle angle was controlled, any readjustment of the subject's knee angle will cause changes in length and pennation angle of the muscle, and potentially change the resulting material property parameter estimates.

In Experiment 2, we demonstrated the effects of isometric contraction on the anisotropic material properties of the gastrocnemius. Results from this experiment indicate that as this activation occurs, the muscle increases its shear stiffness in the direction perpendicular to the fiber direction. Previous studies utilizing MRE for estimation of skeletal muscle during activation, such as works by Zonnino *et al* (2019) and Schrank *et al* (2020), also reported increases in stiffness estimates during isometric contractions. These studies also found greater increases during agonist actions than antagonist actions, with the gastrocnemius functioning as an agonist during plantar-flexion, displaying larger parameter changes than in dorsi-flexion, or antagonist action for the gastrocnemius. Our TI-NLI anisotropic property estimates suggest the increase in stiffness estimated in these previous studies was a result of stiffening of the tissue in the perpendicular direction with little to no increase in

stiffness in the fiber direction during activation. We expect these increases during isometric contraction are a consequence of the cross-bridge model attributed to Huxley (1957), which indicates that cross-bridges are created by myosin and actin bonding, which exert forces along the bridge during bonding that occurs in conjunction with conversion of ATP into ADP. This cross-bridge loading creates lateral stresses between sarcomeres, specifically the z-disc, the region of the muscle fiber linking sarcomeres together, and upon the surrounding collagen supportive structures (Ramaswamy *et al* 2011, Maas 2019). However, the forces are not a constant, as the cross-bridge only spends a portion of time strongly attached to actin. The amount of time these cross-bridges spend attached to actin fibrils increases in response to load. Thus, the cross-bridge 'duty cycle' is high frequency, meaning that MRE likely captures an averaged state of the cross-bridge loading and unloading (Huxley and Simmons 1971, Herzog *et al* 2015).

The two experiments reported here highlight how anisotropic MRE utilizing TI-NLI can be an effective tool for *in vivo* mechanical evaluation of skeletal muscle structural and functional health and agree with mechanical responses of muscle shown in previous $ex\ vivo$ experiments. First, we observed how shear stiffness parallel and perpendicular to muscle fibers, μ_1 and μ_2 , influenced the complex relationship between ϕ and muscle loading. μ_1 correlates with increasing tension caused by muscle lengthening through passive loading, while μ_2 captures the lateral loading across cross-bridges and between sarcomeres and the surrounding collagen-based structures that occurs during isometric contraction. On the other hand, while ζ appears to be a necessary component of the parameter estimation process and shows changes with both passive lengthening and active contraction, ζ is the most common anisotropic material parameter explored in previous $ex\ vivo$ experiments. While the responses of ζ are similar to those of ϕ in these experiments, differences between the two parameters in future experiments could help provide greater insight into tissue behavior.

Muscle under tension not only changes the shape and structure of cells, which are expected to affect tissue mechanics, but also generates significant pre-strain fields which further influence shear wave propagation. Muscle stress fields can be reasonably approximated as having symmetry around an axis along the length of the muscle, so these effects can be adequately modeled by effective parameters of a NITI model (Takaza et al 2013). A simple model of passive stretching produces tensile pre-stress fields along the muscle, and radially symmetric compressive pre-stress perpendicular to the muscle axis due to the Poisson effect (Pietsch et al 2014). This will increase shear wave speed along the muscle axis and perpendicular to the muscle axis, though likely a lesser amount, resulting in an increased apparent anisotropy. Active muscle contraction also has tensile stress along the muscle axis; however, this is generated by shortening the muscle which increases cross-sectional area which gives a tensile pre-strain. This increases wave speed in both directions, giving an increased overall effective stiffness, and lower effective anisotropy. Accurate modeling of these acoustoelastic effects (Abiza et al 2012, Crutison et al 2022, 2022b) requires a nonlinear computational model and knowledge of the both the pre-strain field, requiring the unstressed state to be known, and the nonlinear mechanical properties. As these requirements are difficult to achieve with in vivo imaging, separation of the mechanical property changes from acoustoelastic changes is not currently feasible. Therefore, a small displacement assumption is used in the estimation of 'effective' mechanical properties which consist of the true unstressed properties mixed with the nonlinear acoustoelastic effects from the pre-strain field. These effective properties are altered by both changes in cellular structure and changes in muscle function, so provided conditions are controlled carefully they can provide useful insight into muscle health.

While the methods utilized in this study were effective at capturing the viscoelastic responses of muscle function with MRE, the study had several limitations. While the MRE and DTI scans have standard imaging noise, other biological tissues and structures within the volume create additional noise and discontinuities that may affect outcomes (McGarry et al 2011). These structures include the fibula, major blood vessels, fatty tissue, and muscle fascia, each of which create challenges for MRE, as they introduce model-data mismatch in multiple small ROIs that we sought to minimize by incorporating spatial information in the inversion process. Muscle fatigue also potentially affected outcomes from Experiment 2 that required consistent force generation over a period of time (Fitts 2008, McLester 2012). Experiment 2 was designed using springs that generate a load below 15% mean voluntary contraction for an average human adult, to avoid significant fatigue during the short imaging time, but this threshold is variable from subject to subject and levels of force application were imprecise as no in situ measurements were recorded. One additional limitation is possible differences in assumed fiber direction for anisotropic estimation and the true fiber direction, especially during Experiment 2, as DTI data was not acquired during each isometric contraction condition but rather was acquired at rest and registered to MRE data from active contraction prior to TI-NLI. Recommendations for future studies include a tailored force output requirement based on an individual subject's MVC and a visual feedback system adjusted to each subject's necessary output level so that a participant can maintain the proper level of contraction. Additionally, subject knee and ankle positions in both experiments were relatively well controlled and consistent within an individual subject's data set, however they were unmeasured and could not be accounted for during statistical analysis, and differences between individuals may account for some of the variability in observed outcomes.

5. Conclusions

In this work, we use anisotropic MRE to capture functional effects on muscle mechanics, including passive muscle lengthening and active contraction to the medial and lateral heads of the gastrocnemius. Using TI-NLI, we generated anisotropic material parameter maps and estimated each parameter within the muscle volumes of participants for each of three conditions during each experiment capturing both passive lengthening and active contraction. Anisotropic mechanical parameters exhibited different trends based on the loading condition, and MRE with TI-NLI may allow us to examine healthy functional response of muscle tissue as well as tissue affect by injuries or pathologies, such as cerebral palsy.

Acknowledgments

This study was supported in part by Grants from the National Institutes of Health (R01-EB027577) and the National Science Foundation (CBET-1911683).

Ethical statement

This work with subjects was approved by the University of Delaware Institutional Review Board with protocol number 1730839–1. All work was conducted in accordance with the principles embodied in the Declaration of Helsinki and local requirements. Subjects gave written informed consent to participate in the study and for publication.

Conflict of interest

The authors have no conflicts of interest to disclose.

ORCID iDs

Daniel R Smith https://orcid.org/0000-0001-9594-9734

References

Abiza Z, Destrade M and Ogden R W 2012 Large acoustoelastic effect Wave Motion 49 364-74

Babaei B, Fovargue D, Lloyd R A, Miller R, Jugé L, Kaplan M, Sinkus R, Nordsletten D A and Bilston L E 2021 Magnetic resonance elastography reconstruction for anisotropic tissues *Med. Image Anal.* 74 102212

Basford J R, Jenkyn T R, An K-N, Ehman R L, Heers G and Kaufman K R 2002 Evaluation of healthy and diseased muscle with magnetic resonance elastography *Arch. Phys. Med. Rehabil.* 83 1530–6

Bayly PV and Garbow J R 2018 Pre-clinical MR elastography: principles, techniques, and applications J. Magn. Reson. 291 73-83

Bensamoun S F, Charleux F, Debernard L, Themar-Noel C and Voit T 2015 Elastic properties of skeletal muscle and subcutaneous tissues in duchenne muscular dystrophy by magnetic resonance elastography (MRE): a feasibility study *IRBM* 36 4–9

Biglands J D, Grainger A J, Robinson P, Tanner S F, Tan A L, Feiweier T, Evans R, Emery P and O'Connor P 2020 MRI in acute muscle tears in athletes: can quantitative T2 and DTI predict return to play better than visual assessment? Eur. Radiol. 30 6603–13

Boesch C, Slotboom J, Hoppeler H and Kreis R 1997 *In vivo* determination of intra-myocellular lipids in human muscle by means of localized 1H-MR-spectroscopy *Magn. Reson. Med.* 37 484–93

Böl M 2009 Micromechanical modelling of skeletal muscles: from the single fibre to the whole muscle *Arch. Appl. Mech. 2009 80* 58 57–67 Crutison J and Royston T 2022a The design and application of a diffusion tensor informed finite-element model for exploration of uniaxially prestressed muscle architecture in magnetic resonance imaging *Eng. Comput.* 1 1–16

Crutison J, Sun M and Royston T J 2022b The combined importance of finite dimensions, anisotropy, and pre-stress in acoustoelastography J. Acoust. Soc. Am. 151 2403

Csapo R, Gumpenberger M and Wessner B 2020 Skeletal muscle extracellular matrix—what do we know about its composition, regulation, and physiological roles? a narrative review *Front. Physiol.* 11 253

Debernard L, Robert L, Charleux F and Bensamoun S F 2011 Characterization of muscle architecture in children and adults using magnetic resonance elastography and ultrasound techniques J. Biomech. 44 397–401

Deshmukh S, Subhawong T, Carrino J A and Fayad L 2014 Role of MR Spectroscopy in Musculoskeletal Imaging Indian J. Radiol. Imaging 24 210–6

Díaz-Manera J, Llauger J, Gallardo E and Illa I 2015 Muscle MRI in muscular dystrophies Acta Myol. 34 95-108

Evans C L and Hill A V 1914 The relation of length to tension development and heat production on contraction in muscle *J. Physiol.* **49** 10–6 Feng Y, Okamoto R J, Namani R, Genin G M and Bayly P V 2013 Measurements of mechanical anisotropy in brain tissue and implications for transversely isotropic material models of white matter *J. Mech. Behav. Biomed. Mater.* **23** 117–32

Fitts R H 2008 The cross-bridge cycle and skeletal muscle fatigue J. Appl. Physiol. 104 551-8

Gillies A R and Lieber R L 2011 Structure and function of the skeletal muscle extracellular matrix Muscle Nerve 44 318-31

Gordon A M, Huxley A F and Julian F J 1966 The variation in isometric tension with sarcomere length in vertebrate muscle fibres *J. Physiol.* **184** 170–92

```
Green M A, Geng G, Qin E, Sinkus R, Gandevia S C and Bilston L E 2013 Measuring anisotropic muscle stiffness properties using elastography NMR Biomed. 26 1387–94
```

- Green M A, Sinkus R, Gandevia S C, Herbert R D and Bilston L E 2012 Measuring changes in muscle stiffness after eccentric exercise using elastography NMR Biomed. 25 852–8
- Guidetti M, Lorgna G, Klatt D, Vena P and Royston T J 2019 Anisotropic composite material phantom to improve skeletal muscle characterization using magnetic resonance elastography J. Mech. Behav. Biomed. Mater. 89 199–208
- Guo J, Hirsch S, Scheel M, Braun J and Sack I 2016 Three-parameter shear wave inversion in MR elastography of incompressible transverse isotropic media: application to in vivo lower leg muscles Magn. Reson. Med. 75 1537–45
- Herzog W, Duvall M and Leonard T R 2012 Molecular mechanisms of muscle force regulation: a role for titin? *Exerc. Sport Sci. Rev.* 40 50–7 Herzog W, Powers K, Johnston K and Duvall M 2015 A new paradigm for muscle contraction *Front. Physiol.*, 6 174
- Hiscox L V, Johnson C L, Barnhill E, McGarry M D J, Huston J, van Beek E J R, Starr J M and Roberts N 2016 Magnetic resonance elastography (MRE) of the human brain: technique, findings and clinical applications *Phys. Med. Biol.* 61 R401–37
- Huijing P A 1999 Muscle as a collagen fiber reinforced composite: a review of force transmission in muscle and whole limb *J. Biomech.* 32
- Huxley A F 1957 Muscle structure and theories of contraction Prog. Biophys. Biophys. Chem. 7 255-318
- Huxley A F and Simmons R M 1971 Proposed mechanism of force generation in striated muscle Nature 233 533-8
- Jenkinson M 2003 Fast, automated, n-dimensional phase-unwrapping algorithm Magn. Reson. Med. 49 193–7
- Jenkinson M, Beckmann CF, Behrens TEJJ, Woolrich MW and Smith SM 2012 Fsl Neuroimage 62 782–90
- Johnson C L, McGarry M D J, Gharibans A A, Weaver J B, Paulsen K D, Wang H, Olivero W C, Sutton B P and Georgiadis J G 2013 Local mechanical properties of white matter structures in the human brain *Neuroimage* 79 145–52
- Johnston J H, Kim H K, Merrow A C, Laor T, Serai S, Horn P S, Kim D H and Wong B L 2015 Quantitative skeletal muscle MRI: I. Derived T2 fat map in differentiation between boys with duchenne muscular dystrophy and healthy boys Am. J. Roentgenol. 205 W207–15
- Kalia V, Leung D G, Sneag D B, Grande F, Del and Carrino J A 2017 Advanced MRI techniques for muscle imaging Semin. Musculoskelet. Radiol. 21 459
- Kaufman K R, An K N and Chao E Y S 1989 Incorporation of muscle architecture into the muscle length-tension relationship *J. Biomech.* 22
- Kellis E and Baltzopoulos V 1998 Muscle activation differences between eccentric and concentric isokinetic exercise Med. Sci. Sports Exerc. 30 1616–23
- Kennedy P, Barnhill E, Gray C, Brown C, van Beek E J R, Roberts N and Greig C A 2020 Magnetic resonance elastography (MRE) shows significant reduction of thigh muscle stiffness in healthy older adults *GeroScience* 42 311–21
- Kennedy P, Macgregor L J, Barnhill E, Johnson C L, Perrins M, Hunter A, Brown C, van Beek E J R and Roberts N 2017 MR elastography measurement of the effect of passive warmup prior to eccentric exercise on thigh muscle mechanical properties J. Magn. Reson. Imaging 46 1115–27
- Komi P V and Viitasalo J H T 1976 Signal characteristics of EMG at different levels of muscle tension Acta Physiol. Scand. 96 267-76
- Litwiller D V, Mariappan Y K and Ehman R L 2012 Magnetic resonance elastography Curr. Med. Imaging Rev. 8 46-55
- Maas H 2019 Significance of epimuscular myofascial force transmission under passive muscle Conditions J. Appl. Physiol. 126 1465-73
- Maganaris C N 2003 Force-length characteristics of the in vivo human gastrocnemius muscle Clin. Anat. 16 215-23
- Mariappan Y K, Glaser K J and Ehman R L 2010 Magnetic resonance elastography: a review Clin. Anat. 23 497-511
- Marty B and Carlier P G 2019 Physiological and pathological skeletal muscle T1 changes quantified using a fast inversion-recovery radial NMR imaging sequence Sci. Rep. 9 6852
- McGarry M et al 2021 A heterogenous, time harmonic, nearly incompressible transverse isotropic finite element brain simulation platform for Mr elastography *Phys. Med. Biol.* 66 055029
- McGarry M et al 2022 Mapping heterogenous anisotropic tissue mechanical properties with transverse isotropic nonlinear inversion MR elastography Med. Image Anal. 78 102432
- McGarry M, Johnson C L, Sutton B P, Van Houten E E, Georgiadis J G, Weaver J B and Paulsen K D 2013 Including spatial information in nonlinear inversion MR elastography using soft prior regularization *IEEE Trans. Med. Imaging* 32 1901–9
- $McGarry\,M\,D\,J, Van\,Houten\,E\,E\,W, Perriñez\,P\,R, Pattison\,A\,J, Weaver\,J\,B\, and\,Paulsen\,K\,D\,2011\,An\,octahedral\,shear\,strain-based\,measure\,of\,SNR\,for\,3D\,MR\,elastography\,Phys.\,Med.\,Biol.\,56\,N153-64$
- McLester J R 2012 Muscle contraction and fatigue Sport. Med. 23 287–305
- Mohammadkhah M, Murphy P and Simms C K 2018 Collagen fibril organization in chicken and porcine skeletal muscle perimysium under applied tension and compression *J. Mech. Behav. Biomed. Mater.* 77 734–44
- Murphy W A, Totty W G and Carroll J E 1986 MRI of normal and pathologic skeletal muscle Am. J. Roentgenol. 146 565–74
- Naruse M, Trappe S and Trappe T A 2022 Human skeletal muscle size with ultrasound imaging: a comprehensive review *J. Appl. Physiol.* 132 1267–79
- Oudeman J, Nederveen A J, Strijkers G J, Maas M, Luijten P R and Froeling M 2016 Techniques and applications of skeletal muscle diffusion tensor imaging: a review J. Magn. Reson. Imaging 43 773–88
- Palnitkar H, Reiter R O, Majumdar S, Lewis P, Hammersley M, Shah R N, Royston T J and Klatt D 2019 An investigation into the relationship between inhomogeneity and wave shapes in phantoms and *Ex vivo* skeletal muscle using magnetic resonance elastography and finite element analysis *J. Mech. Behav. Biomed. Mater.* 98 108–20
- Pietsch R, Wheatley B B, Donahue T L H, Gilbrech R, Prabhu R, Liao J and Williams L N 2014 Anisotropic compressive properties of passive porcine muscle tissue *J. Biomech. Eng.* 136 11
- Pillen S and van Alfen N 2011 Skeletal muscle ultrasound Neurol. Res. 33 1016-24
- Raiteri B J, Hug F, Cresswell A G and Lichtwark G A 2016 Quantification of muscle co-contraction using supersonic shear wave imaging I. Biomech. 49 493–5
- Ramaswamy K S, Palmer M L, Van Der Meulen J H, Renoux A, Kostrominova T Y, Michele D E, Faulkner J A, Faulkner J A and Michele D E 2011 Lateral transmission of force is impaired in skeletal muscles of dystrophic mice and very old rats *J. Physiol.* 589 1195–208
- Riemann B L, DeMont R G, Ryu K and Lephart S M 2001 The effects of sex, joint angle, and the gastrocnemius muscle on passive ankle joint complex stiffness *J. Athl. Train.* **36** 369
- Ringleb S I, Bensamoun S F, Chen Q, Manduca A, An K-N and Ehman R L 2007 Applications of magnetic resonance elastography to healthy and pathologic skeletal muscle J. Magn. Reson. Imaging 25 301–9
- Schrank F, Warmuth C, Görner S, Meyer T, Tzschätzsch H, Guo J, Uca Y O, Elgeti T, Braun J and Sack I 2020 Real-time MR elastography for viscoelasticity quantification in skeletal muscle during dynamic exercises Magn. Reson. Med. 84 103–14

- Schwenzer N F, Steidle G, Martirosian P, Schraml C, Springer F, Claussen C D and Schick F 2009 Diffusion tensor imaging of the human calf muscle: distinct changes in fractional anisotropy and mean diffusion due to passive muscle shortening and stretching NMR Biomed. 22 1047–53
- Shen W, Gong X, Weiss J and Jin Y 2013 Comparison among T1-weighted magnetic resonance imaging, modified dixon method, and magnetic resonance spectroscopy in measuring bone marrow fat *J. Obes.* 2013 298675
- Sinha S, Sinha U and Edgerton V R 2006 *In vivo* diffusion tensor imaging of the human calf muscle *J. Magn. Reson. Imaging* 24 182–90 Smith D R *et al* 2022 Anisotropic mechanical properties in the healthy human brain estimated with multi-excitation transversely isotropic Mr elastography *Brain Multiphys.* 3 100051
- Smith DR, Guertler CA, Okamoto RJ, Romano AJ, Bayly PV and Johnson CL 2020 Multi-excitation magnetic resonance elastography of the brain: wave propagation in anisotropic white matter *J. Biomech. Eng.* 142 51–9
- Stecco C, Pirri C, Fede C, Yucesoy C A, De Caro R and Stecco A 2021 Fascial or muscle stretching? a narrative review *Appl. Sci.* 11 1–11 Takaza M, Moerman K M, Gindre J, Lyons G and Simms C K 2013 The anisotropic mechanical behaviour of passive skeletal muscle tissue subjected to large tensile strain *J. Mech. Behav. Biomed. Mater.* 17 209–20
- Tweten D J, Okamoto R J and Bayly P V 2017 Requirements for accurate estimation of anisotropic material parameters by magnetic resonance elastography: a computational study Magn. Reson. Med. 78 2360–72
- Tweten DJDJ, Okamoto RJ, SchmidtJL, Garbow JR and Bayly PV 2015 Estimation of material parameters from slow and fast shear waves in an incompressible, transversely isotropic material *J. Biomech.* 48 4002–9
- van Hooren B, Teratsias P and Hodson-Tole E F 2020 Ultrasound imaging to assess skeletal muscle architecture during movements: a systematic review of methods reliability, and challenges J. Appl. Physiol. 128 978–99
- Wheatley B B 2020 Investigating passive muscle mechanics with biaxial stretch Front. Physiol. 11 1021
- Yao L, Yip A L, Shrader J A, Mesdaghinia S, Volochayev R, Jansen A V, Miller F W and Rider L G 2016 Magnetic resonance measurement of muscle T2, fat-corrected T2 and fat fraction in the assessment of idiopathic inflammatory myopathies Rheumatology (Oxford) 55 441
- Zonnino A, Smith D R, Delgorio P L, Johnson C L and Sergi F 2019 MM-MRE: a new technique to quantify individual muscle forces during isometric tasks of the wrist using Mr elastography *IEEE Int. Conf. Rehabil. Robot. (Toronto, ON, 24–28 June 2019)* (Picastaway, NJ: IEEE) pp 270–5